Magnetoconductance of a nanoscale antidot

A. S. Sachrajda and Y. Feng
Institute for Microstructural Science, National Research Council, Ottawa, Canada K1A 0R6

R. P. Taylor
Institute for Microstructural Science, National Research Council, Ottawa, Canada K1A 0R6
and School of Physics, University of New South Wales, Sydney, New South Wales 2052, Australia

G. Kirczenow
Department of Physics, Simon Fraser University, Burnaby, British Columbia, Canada V5A 1S6

L. Henning, J. Wang, P. Zawadzki, and P. T. Coleridge
Institute for Microstructural Science, National Research Council, Ottawa, Canada K1A 0R6
(Received 26 January 1994; revised manuscript received 9 June 1994)

A 300-nm-diameter gate is used to introduce an antidot or artificial impurity into a quantum wire defined in an $Al_xGa_{1-x}As/GaAs$ two-dimensional electron gas. At low magnetic fields, geometry-induced quantum interference effects are observed, while at higher fields adiabatic edge-state transport is established. In the transitional regime, conductance resonances due to magnetically bound impurity states exhibit distinct characteristics including beating, sharp period changes, and spin splitting. An asymmetry is observed between the resonances observed as a function of magnetic field and gate voltage. The results are explained by a model based on an interedge-state coupling mechanism.

I. INTRODUCTION

In this paper, we employ a recent fabrication technique[1] to independently bias the 300-nm-diameter central gate of the device in Fig. 1. Each of the five gates can be separately addressed, allowing different geometries to be defined in the two-dimensional electron gas (2DEG) at the $Al_xGa_{1-x}As/GaAs$ interface. In the experiments presented, a set of two diagonally opposite gates, e.g., gates two and four, are switched off by shorting them to the 2DEG. Biasing gates one and three then define a quantum wire and by tuning the central-gate bias (V_g) the geometry evolves into an antidot positioned between two parallel constrictions. The potential inhomogeneity under the central gate can also be viewed as a well-defined artificial impurity (AI) introduced at a known location. Motivated by the fundamental role played by impurities in the electronic transport through mesoscopic semiconductor systems, we have studied the behavior of the artificial impurity over a range of magnetic fields.[2] At low magnetic fields, the impurity shapes the classical electron trajectories (Sec. II), while at higher fields, the magnetoresistance is determined by edge states bound to the impurity. The coupling process, which links the transmitted and bound edge states, is studied as a function of both magnetic field (Secs. III–V) and central-gate bias (Sec. VI). To check for the reproducibility of the effects, the device was cooled using a dilution refrigerator on four occasions and in each case measurements were made after various amounts of illumination with a red light-emitting diode (LED). After the wafer was illuminated to saturation, the electron density and electron mobility of the bulk 2DEG were 3.5×10^{11} cm^{-2} and 1.5×10^{6} cm^2/Vs, respectively.

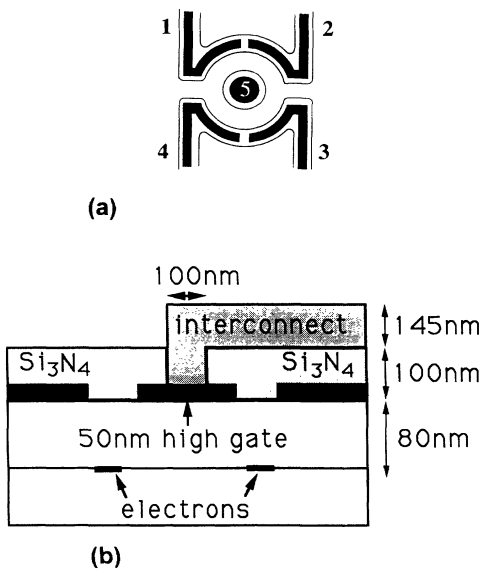

FIG. 1. (a) A schematic representation of the gate pattern is shown. To contact gate five, we adopt the two-level metallization architecture shown in (b).

II. LOW MAGNETIC-FIELD CHARACTERIZATION

At low magnetic fields, the classical electron trajectories form closed loops around the artificial impurity. The cyclotron diameter is greater than that of the antidot. For a given loop, the magnetic flux threaded through

the enclosed area A determines the quantum interference of the partial waves associated with the trajectories. A simple flux argument reveals a transmission that oscillates with a characteristic period ΔB given approximately by the Aharonov-Bohm (AB) formula, $\Delta B = h/eA$.[3] Although the impurity does not define a perfect ring, the spread in A is sufficiently limited for the magnetoresistance to be dominated by a single period over a small region of magnetic field. This is shown in Fig. 2 where reproducible oscillations, superimposed on the classical resistance background, emerge for biases at which the region under the central gate is depleted. The oscillations persist up to 4 K, with a $T^{-1/2}$ amplitude dependence.

The diameter extracted from the AB formula is a measure of the average trajectory diameter around the impurity. In a simple approximation, this is equal to (DI + DO)/2. DI and DO are the inside and outside diameters of the conducting region around the impurity. Calculations of A reveal an average trajectory diameter of 610 nm for the minimum biases required for depletion under the gates. This is consistent with values for the average width of the wire and diameter of the antidot (DO $\approx$ 900 nm $- d_0$ and DI $\approx$ 300 nm $+ d_i$), calculated from the lithographic dimensions and lateral depletion distances d_0 and d_i of the gates. The device construction allows DO and DI to be independently tuned. This is demonstrated in the insets of Fig. 2. The average trajectory diameter, calculated from ΔB can be reduced, or increased, by tuning the wire gates (upper inset) or central gate (lower inset), respectively. At the minimum biases required for depletion, approximate estimates for DI and DO are 400 and 800 nm and we might therefore anticipate controlled variations in the conducting channel diameter of 400 nm. However, experimentally we find there is an extra limitation. The AB oscillations disappear when the conductance of either of the two constrictions, formed by the artificial impurity and the wire wall, is reduced to slightly above $2e^2/h$. Since the gate action used to reduce the conductance also decreases the electron density, we speculate that this effect may be an artifact related to the lower electron density in the constrictions increasing the roughness of the potential profile in the constrictions.[4] This will reduce the electronic phase coherence. This effect limits controlled variations in the average diameter to between 540 and 680 nm.

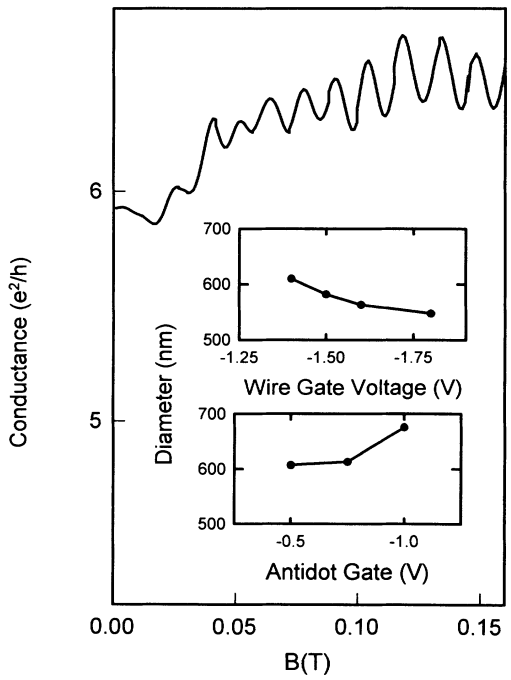

FIG. 2. The magnetoresistance taken at 50 mK, which shows Aharonov-Bohm oscillations induced by the antidot. The insets demonstrate how the diameter of the trajectory loops, deduced from the oscillation period, can be altered by tuning various gate voltages (see text for details).

Finally, we note that at these low fields, the measured device conductance is very close to the classical addition of the conductances of the two individual constrictions (i.e., as measured with the second constriction pinched off).[5] We have observed no evidence for mode locking of the two constrictions.[6,7]

III. MAGNETORESISTANCE THROUGH TWO PARALLEL CONSTRICTIONS: THE ROLE OF INTEREDGE STATE COUPLING

At magnetic fields sufficient for edge-state transport, a range of experiments have previously considered the case of two constrictions arranged in series[8] and in parallel.[7,9] We have investigated the situation of two parallel potential barriers with the advantage that each of the barriers can be individually tuned and even pinched off. The magnetic-field range spanned the transition from nonadiabatic to adiabatic edge-state transport.

The two parallel constrictions L and R, formed between the impurity and the wire's walls, each feature a potential barrier as described above. Figure 3(a) shows measurements at 3.3 T, corresponding to two spin-unresolved edge states occupied in the bulk 2DEG. Sufficient bias is applied to deplete under the antidot gate. The side gate is tuned to pinch off constriction R. Curve (i) is then generated by sweeping the other side-gate bias. The conductance plateau, at $2e^2/h$, corresponds to one spin-unresolved edge state fully transmitted through constriction L. In curve (ii), the same gate bias is swept but with constriction R set to transmit one edge state. At gate biases for which both constrictions have individual conductances G_R and G_L of $2e^2/h$, the total conductance is also accurately equal to $2e^2/h$. For this device configuration, there is also an edge state circulating round the antidot. At higher negative voltages in curve (ii), when constriction L is pinched off, the device conductance G_T remains equal to $2e^2/h$. The origin of this behavior lies in the adiabatic transport of edge states. In this regime, the mode circulating the antidot does not couple to the modes that are transmitted or reflected at the barriers and hence does not affect their transmission coefficients. On depleting constriction L, the current carrying mode, which had been transmitted through the L constriction, switches to the R constriction, but since its

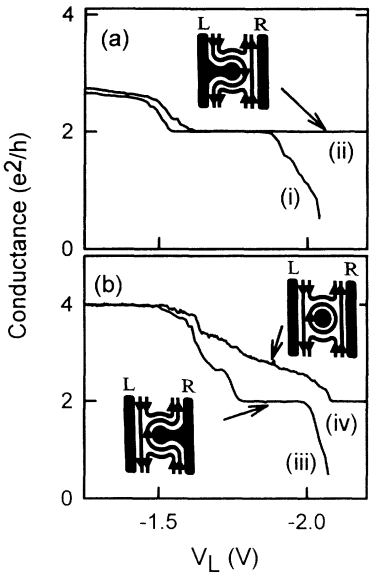

FIG. 3. The total conductance of the antidot taken as a function of the bias applied to gate L. At 3.3 T (corresponding to two spin-unresolved edge states in the bulk), G_R is set to transmit zero (i) and one (ii) spin-unresolved edge state. At 2.2 T (corresponding to three spin-unresolved edge states in the bulk), G_R is set to transmit zero (iii) and one (iv) spin-unresolved edge states. $T=50$ mK for all traces. The insets are schematics of the edge states at various points on the curve [N.B. in (b) one of the two edge states reflected at the antidot is omitted for clarity].

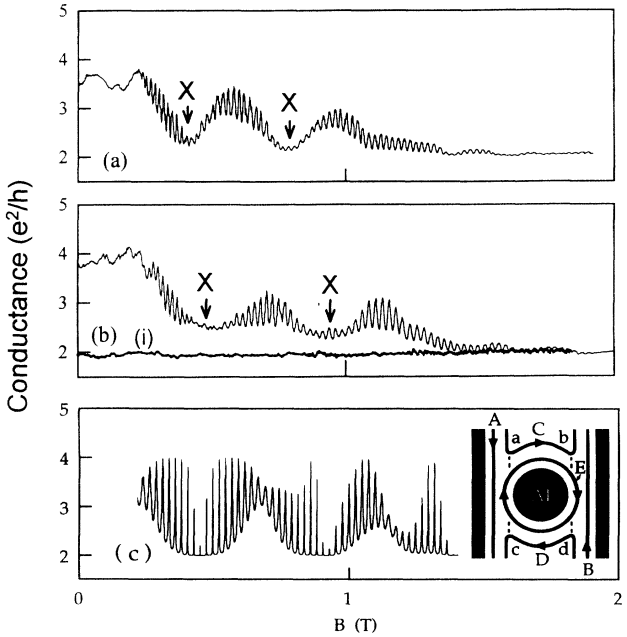

FIG. 4. (a) and (b) The conductance of the antidot on two cooldowns, each taken at 50 mK. X marks the period change. (c) Results and schematic representation of the theoretical model involving interedge-state coupling. Curve (i) shows the magnetoconductance when the voltage on one of the wire gates is adjusted to pinch off that side (see text).

transmission coefficient through the antidot region remains at one, the device conductance remains at $2e^2/h$.

As the magnetic field is lowered, there are two scenarios for how this adiabatic picture might breakdown. For simplicity we maintain the case of the two conductances G_R and G_L set close to $2e^2/h$. As the magnetic field is lowered, the number of fully transmitted edge states therefore remains set at one, while the number reflected at the two barriers increases. One possible mechanism is shown in the inset to Fig. 4(c). Coupling has been introduced between the reflected edge states (C and D) and the state bound to the antidot (E). A fraction of the current carried by the reflected state is transmitted at the antidot and the net effect of the coupling is to increase G_T above $2e^2/h$. This mechanism requires coupling between edge states with different Landau-level indices. In a high electron mobility sample, this coupling should be induced by the geometry of the depletion potential (rather than random defects). Thus, it is reasonable to make the assumption (ignoring other effects such as differences in the spatial separation of the modes along the antidot edge) for the purpose of the model that the coupling is strongest near the openings of the constrictions, points a, b, c, and d, where this potential has the most structure, i.e., is most rough.[10] Alternatively, coupling might exist between edge states with identical Landau-level indices—between the transmitted edge states (A and B) and the bound state (E)—causing G_T to decrease below $2e^2/h$. This is reminiscent of the mechanism proposed by Jain and Kivelson[9] to explain impurity-induced breakdown of the quantum Hall effect. It has been discussed theoretically by Kirczenow[10] and Büttiker.[11]

The primary mechanism for our device is revealed in Fig. 3(b). Curve (iii) is a plot of the conductance through the device with $G_R=0$. The accuracy of the plateau conductance suggests no coupling at these fields and gate voltages between the edge states at the two constriction edges of constriction L. In curve (iv), G_R is set to $2e^2/h$. For biases of gate L sufficient to pinch off constriction L, the total conductance is again accurately equal to $2e^2/h$. This confirms that in constriction R there is also negligible coupling between the edge states at the two edges. Yet for biases where both constrictions have individual conductances of $2e^2/h$, then $G_T > 2e^2/H$. This behavior is only consistent with the forward-scattering mechanism shown in the Fig. 4(c) inset, and is in contrast to Ref. 12. It is interesting to note that the equivalent coupling between edge states with different Landau-level indices has also been shown to be the dominant mechanism in certain quantum-dot geometries,[13] and present in others.[14,15] where edge states are bound by the confining perimeter of the dot rather than by an artificial impurity. We will return to this comparison with dots in Sec. V.

IV. TRANSMISSION RESONANCES IN THE MAGNETOCONDUCTANCE

In Figs. 4(a) and 4(b) the field is swept from 0 to 2 T for two cooldowns. The gates were set such that, when mea-

sured independently, G_L and G_R remained at $2e^2/h$ throughout this field range. Even though the confinement changes from purely electrostatic at zero field to mainly magnetic at 2 T, the number of (spin-unresolved) conduction modes in each constriction remains one. G_L and G_R, therefore, remain at $2e^2/h$. Curve (i) of Fig. 4(b) shows the magnetoconductance of one constriction (with the other pinched off) to be $2e^2/h$ throughout the range. A calculation for the electron density in the constrictions shows that this only requires the constriction width to be less than 100 nm. By monitoring G_T, we can observe how parallel constrictions behave as a function of field. At zero field G_L and G_R add classically (in Fig. 4(a) and 4(b), G_T is close to $4e^2/h$ at zero field). Between 0.3 and 3 T, we observe the transition to adiabatic transport (with $G_T \approx 2e^2/h$ at higher fields). In this transitional regime, when the forward-scattering mechanism operates, magnetoconductance oscillations are observed. Periodic oscillations have been observed in other multiply connected nanostructures,[7-9] but abrupt period changes (described below) and the very clear beatlike structures have not.[16] These new characteristics have been observed on four cooldowns[17] and are believed to be intrinsic to the device. We now explain the features in terms of resonant scattering of electrons between the states C and D through the discrete energy levels of the bound state E.

The experiments outlined in Sec. III show the predominant coupling to be the forward-scattering mechanism shown in the inset to Fig. 4(c). Furthermore, for both possible coupling mechanisms, calculations of the conductance using a generalization[10] of the scattering theory described in Ref. 15 reveal that the features of the experiment can only be explained by the forward-scattering mechanism. In these calculations, the transmission T_{CD} between the edge states C and D was evaluated from the interedge-state scattering probabilities T_a, T_b, T_c, T_d, and the phase shifts accumulated by the electron wave function in going round every possible closed orbit around the antidot. These orbits are E and every other closed orbit that can be constructed out of E, C, and D, and the scattering events a, b, c, and d that link C and D to E. The Landauer form of the two terminal conductance $G_T = 2e^2/h\,(1+T_{CD})$ was then used for a comparison with the magnetoconductance obtained in the experiments. In Fig. 4(c), the theory closely matches the main features of the experiment especially when allowance is made for dampening effects, such as kT smearing and inelastic scattering, which were excluded from the calculations.[10] The beating effect is a manifestation of the interference between different orbits of the antidot. The theoretical beat pattern's lower envelope can be matched to that of Fig. 4(a) or 4(b) by increasing and decreasing the coupling strength, respectively. The AB formula can be used to extract a diameter from the oscillation period in a similar way to that used at low fields. In this regime, however, the period corresponds to the addition of a flux quantum inside the area enclosed by the mode circulating the antidot and the diameter (typically $\sim$480 nm) is, therefore, smaller than that obtained in Sec. II.

Figures 4(a) and 4(b) exhibit abrupt increases (5 to 15%) in the period, ΔB, when B increases past certain values. This is in contrast to the almost constant period in the calculations of Fig. 4(c). The location of the increases is marked by X's. In Figs. 4(a) and 4(b), the jumps occur at nodes in the beat pattern. This was not always the case. On different cooldowns and after different LED illuminations, they occurred at various places along the beat pattern, including the antinode or between the antinode and node. We conclude that the beats and period changes are different phenomena. This is seen in Fig. 5 where oscillations are shown over small ranges where the period change occurs. At fields below the transition, the oscillations' maxima align with the grid. In Fig. 5(a), after a missing oscillation, the minima align with the grid and the behavior initially appears to resemble the π phase shift recently observed.[12] However, further to the right the minima cease to match the grid lines, confirming that the period is changing and not just the phase. In Fig. 5(b), we show a second case where at fields slightly higher and lower than the transition region, the oscillations are in phase. This results in a few slightly larger amplitude oscillations. Other experiments, see, for example, Fig. 5(c), showed that these two cases are not typical and that the two periods may overlap over a narrow field range with no simple phase relationship at the transition.

We now suggest a picture that explains this phenomenon. Whereas there are several possibilities to explain a decrease in period as the magnetic field is increased, we have found no simple explanation for the observed increase in period. Inadequate explanations include (i) a change in the enclosed area due to an inhomogeneous potential—this would always result in an increased area and therefore decreased magnetic-field period; (ii) a change in the enclosed area due to a magnetic-field variation in the spatial location of the edge-state wave functions (calculations show that due to the finite size of the edge-state wave function, the period changes are more gradual than those observed); (iii) magnetic-field period changes associated with the beating phenomena (these effects are included in the calculations but are found to be inconsistent with the observed period-change behavior); (iv) a variety of coupling

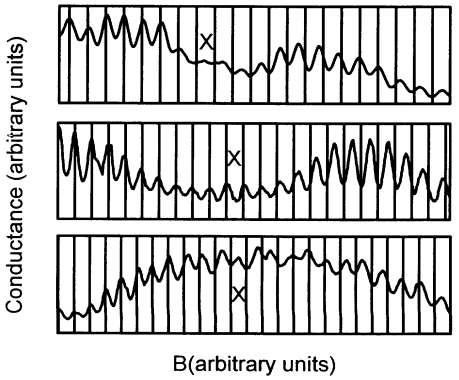

FIG. 5. Detailed plots of three different period changes demonstrating that the period changes marked by X can occur at different locations within the background beat pattern. $T \sim 50$ mK.

schemes between the edge state circulating around the antidot and a second natural inhomogeneity were considered but none of the calculations was able to reproduce the data. However, it is found that a second inhomogeneity can explain the period change under the following circumstances. A local maximum in the potential energy, labeled X in inset (a) of Fig. 6, induces a local maximum in the energy of a particular Landau level (or more precisely, in the spectrum of a magnetoelectrostatic subband). As the magnetic field increases, eventually this maximum rises above the Fermi energy, and the local maximum at X supports a new edge state Y. The formation of Y has a dramatic effect on the values of B at which edge state E comes into resonance and this changes ΔB. However, this is not due to a change in A. This is demonstrated in insets 6(d) and 6(e), where the calculated electron eigenfunctions do not show a significant position change. The calculations were performed for the annulus geometry shown in 6(b), using the model potential-energy function shown in 6(c). The calculated change in period shown in 6(f) results from a nonlocal effect arising from the conservation of particle number $N=2(l_E-l_Y+l_{Y'}-l_A)$ in the annulus, where l_i is the azimuthal quantum number of the state i. This dependence of l_E on l_Y leads to a sudden change in ΔB as Y is formed. For our experimental situation [Fig. 6(a)] Y forms in a smaller region near E. The phase shift that E acquires in the vicinity of X will be similarly affected by *local* conservation of charge leading to an analogous period change but of a smaller magnitude. More than one potential maximum could be present in the vicinity of the central gate[4] and we postulate that two such maxima give the observed changes in period observed in Fig. 4.[4] Further details of this model can be found elsewhere.[2]

V. SPIN-RESOLVED EDGE STATES

At higher magnetic fields, it is possible to resolve resonances originating from edge states with different spin. For this regime it is instructive to compare quantum dot[13] and antidot systems. For the dot geometry, the potential barriers are located at the entrance and exit of the dot. For both geometries, experiments are modeled by an interedge-state coupling mechanism operating at the sites at which the edge-state curvature is a maximum.[10,15] For the dot geometry, the transmission is decreased at resonance while in contrast it is enhanced for the antidot geometry.[10]

High magnetic-field experiments on quantum dots reveal the two series of resonances to be locked in exact antiphase (resonances from one spin species occur exactly half way between the neighboring resonances of the second spin species).[13] The first qualitative explanation of this behavior included electron-electron interactions within the backscattering process.[18] In this picture the addition spectrum is dominated by the electron interaction rather than the single electron level spacing. Models have since been developed in terms of an effective capacitance between the bound and transmitted edge states.[19,20]

For the more open antidot geometry, similar effects have now been observed in the sequence of experiments shown in Fig. 7 and by others.[12] At the low fields in Fig. 7(a), the oscillations have an almost constant period (as described in Sec. IV). Splitting in the resonances occur at the higher fields shown in the inset of Fig. 7(b). At still higher fields, the spin-splitting increases until in Fig. 7(b) we observe a region of uniform amplitude oscillations, but with a period half that observed in Fig. 7(a). Exhibit-

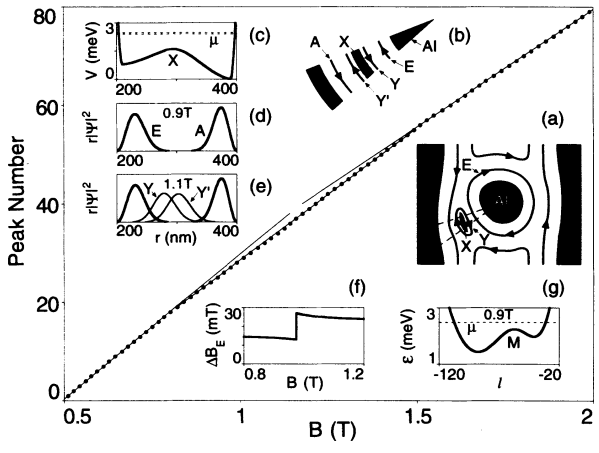

FIG. 6. Position of conductance peaks. Lines are a guide to the eye. Breaks are period changes. (a) Schematic of artificial impurity AI, local potential-energy maximum X, and edge state Y that forms around it. (b) Region between dashed lines in (a) approximated by sector of annulus. (c) Model potential energy used. Upper (lower) dashed line is Fermi energy at 0.9 (1.1) T. (d) Edge states before Y forms. Labels as in (b). (e) States after Y forms. (f) Period of bound state E for geometry of complete annulus. (g) Energy spectrum exhibits maxon M.

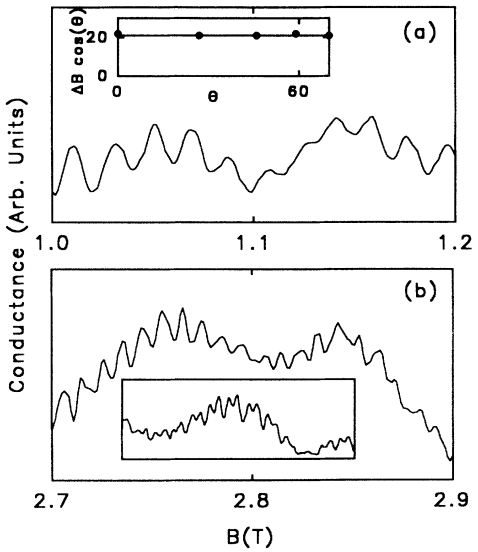

FIG. 7. Magnetic-field sweeps showing the halving of the oscillation period between (a) low magnetic-field regimes and (b) high magnetic-field regimes. The inset to (b) is taken at an intermediate field range period b just sufficient to achieve spin resolution of the edge states. The inset to (a) shows the normalized oscillation period vs the tilt angle (see text).

ing similar behavior to quantum dots, the two series of resonances (from the two spin species) are locked in exact antiphase. The oscillations remain in this mode until the higher fields of the adiabatic regime are reached, where the interedge-state coupling mechanism responsible for the resonances is effectively switched off and, accordingly, conductance oscillations are no longer observed. The magnetic-field range from when the spin splitting is first observed to the adiabatic regime was narrow, typically from approximately 2 to 3 T.

In an attempt to increase the spin splitting at fields below the transition to the adiabatic regime, the magnetic field was tilted. The locking was found to occur at all tilts, and the period of the oscillations scaled simply with the normal component of the tilt. An example is shown in the inset of Fig. 7(a). The normalized period (the period multiplied by $\cos\theta$ where θ is the tilt angle) is plotted for oscillations of the same spin species. This normalized period is independent of tilt angle. The resonances of the two spin species are, therefore, not determined by a simple Zeeman term (which is related to the total component of the magnetic field). Instead, the locking phenomenon is thought to result from electron interaction, in a similar way to the dynamics of quantum dots,[13,18–20] although it should be stressed that the period of the individual spin species resonances is in agreement with that deduced from the area enclosed by the mode encircling the antidot.

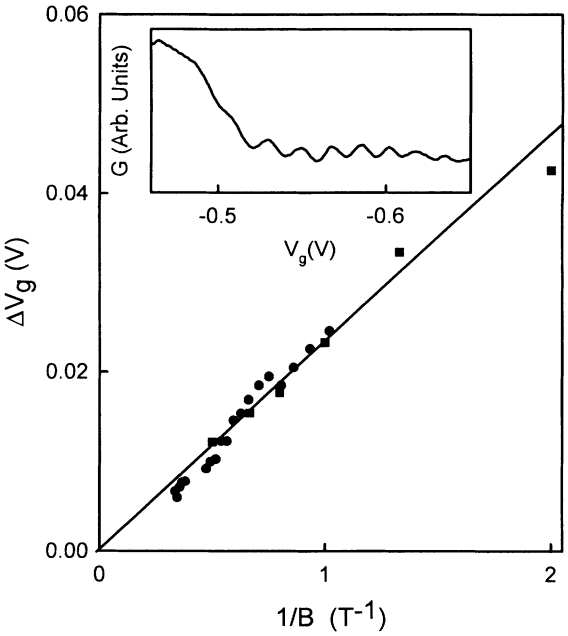

FIG. 8. Conductance oscillations generated by sweeping the bias applied to the antidot gate. The inset shows a typical trace taken at 1.3 T and 50 mK showing the resonance oscillations associated with the $G=2e^2/h$ plateau. The main plot shows the reciprocal relationship between the period and the magnetic fields at which the traces were taken. The circles and squares are for data taken on two separate occasions.

VI. GATE-VOLTAGE-INDUCED RESONANCES

Resonances associated with the impurity-bound states can also be detected as the size of the impurity is changed. The device allows a clear demonstration of this effect since V_g the bias applied to central gate can be adjusted independently of the outer gate biases. In the inset of Fig. 8, V_g is swept as the two outer gate voltages and field are kept constant. Resonances are evident around the plateau. Consider the gate-voltage period ΔV_g in more detail. In the absence of electron-electron interaction effects, one would expect ΔV_g to be determined by $\Delta A = h/eB$. For small changes, A varies as $2\pi r \Delta r$, where r is the radius of the impurity. Assuming $\Delta r \propto \Delta V_g$, we obtain $\Delta V_g \propto 1/B$. Figure 8 shows the linear relationship for two typical cooldowns. At a field of 2 T, ΔV_g corresponds to $\Delta r = 1.5$ nm.

Regimes exist where oscillations occur as a function of field but not as a function of V_g. This reproducible effect is illustrated in Fig. 9. The mean conductance [Fig. 9(a)] and oscillation amplitude [Fig. 9(b)] are plotted as a function of field. The field sweep (circles) corresponds to $V_g = -0.55$ V. The data represented by triangles was compiled from a range of V_g sweeps taken at constant field between 1 and 3 T. The curves in Fig. 9(a) show a close agreement in the beat pattern. Minor deviations are attributed to a slight rearrangement of traps (induced by the many V_g sweeps), which perturb the device potential profile and hence the beat pattern. Deviations also result from the presence of the oscillations on top of the beat pattern, which contribute an uncertainty equal to their

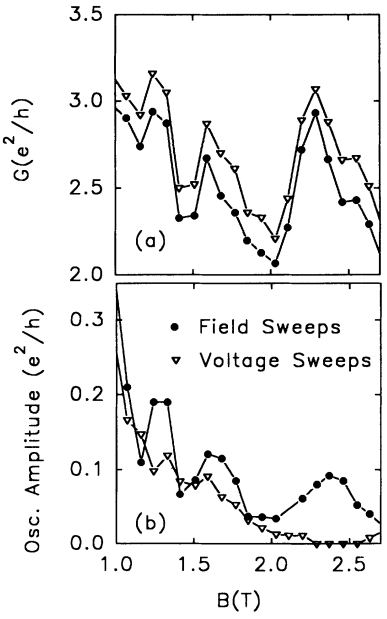

FIG. 9. A comparison of the conductance generated by sweeping magnetic field (circles) and antidot gate voltage (squares). The former is generated by sweeping magnetic field for fixed $V_g = -0.5$ V, while the latter is compiled from a range of V_g sweeps taken at constant magnetic field between 1 and 3 T. (a) shows the background conductance to be similar while (b) shows the behavior in oscillation period to be distinctly different. $T \sim 50$ mK for all traces.

amplitude. Allowing for these small perturbations, the beat patterns of the two curves are almost identical. In contrast, Fig. 9(b) reveals the oscillations' amplitudes, extracted from the same set of field and V_g sweeps, to have distinctly different behavior for the two traces. In the field sweep, the oscillation amplitude increases on the peaks (antinodes) of the beats, whereas this amplitude modulation is small or nonexistent for the V_g sweeps. In fact, oscillations are completely absent on the third beat of data extracted from the V_g sweeps. Further experiments will be required to develop a rigorous model, however, here we suggest an explanation that is in qualitative agreement with the observations.

Broadening of the oscillations is determined by the finite lifetime of the electrons in the bound state. This is limited by both inelastic scattering events and an intrinsic leakage of electrons at the coupling points *a* to *d* [see inset of Fig. 4(c)]. The latter effect increases the broadening of the oscillations at the antinodes of the peaks. When V_g is swept, an additional broadening mechanism may become operative. As V_g is swept, the electron distribution in the doped $Al_xGa_{1-x}As$ layer readjusts to achieve equilibrium and a smooth electrostatic potential. The time constant of this process is not known, although several seconds is reasonable (for example, after illumination with a LED, 20 s is typical to reestablish a constant resistance). A retrospective comparison of this time constant with the gate sweep rate suggests the electrostatic potential may be slightly out of equilibrium and, therefore, spatially rough in comparison with the field sweeps. This roughness is increased in narrow regions because of the reduced screening by the 2DEG (electron redistribution can reduce this effect, but only for time constants longer than those discussed here).[4] The roughness will, therefore, be most apparent in the narrow regions between the wire edges and impurity. The roughness will be minimal in the region between *a* and *b* (and between *c* and *d*) and phase coherence across these regions will be maintained. Interference between the pair of paths an electron can take through each one of these regions is responsible for the formation of the envelope of the beat pattern.[10] Thus it is consistent that the beat-pattern envelope is almost undiminished in the V_g sweeps (compared with the field sweeps) while the Aharonov-Bohm oscillations (which require phase coherence around the entire orbit *E*, including the rougher regions between the antidot and the wire walls) are strongly damped. This damping is greatest at the antinodes of the beat pattern where the lifetimes of an electron in the Aharonov-Bohm resonant states are the shortest.

Figure 10 shows the smearing of the beats as the temperature is raised. The data is taken for temperatures above those required to observe the resonances associated with the single electron energy levels of the bound state (<600 mK). Three major beats are apparent in the field range. The beats at higher fields are more smeared by raising the temperature than those at lower fields. Our estimates (which involve some extrapolation) for the smearing temperatures T^* (i.e., the temperatures at which the beats would not be apparent) are 14 K for beat 1 and 8 K for beat 3. This can be explained qualitatively

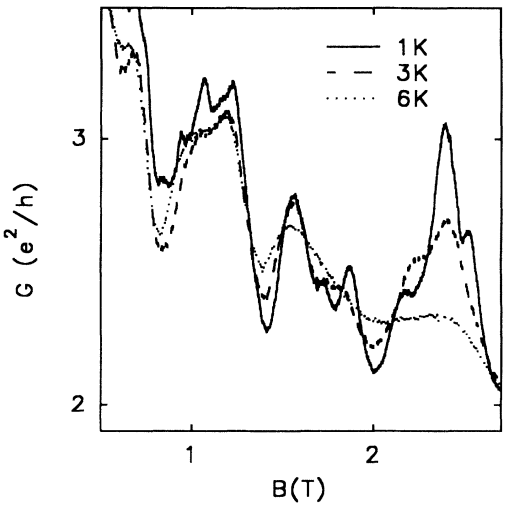

FIG. 10. The temperature dependence of the beat pattern.

by a model by Kirczenow[10] in which the smearing temperature T^* is given by

$$kT^* = \xi |\delta(l_1 - l_2)/\delta\epsilon|^{-1} , \quad (1)$$

where l_1 and l_2 are the azimuthal eigenvalues of the innermost edge state and its nearest neighbor at the Fermi energy, ϵ is the energy, and ξ is a constant close to one. The origin of the field dependence of the smearing temperature is an increase and eventual divergence of $|\delta l_2/\delta\epsilon|$ as the second Landau level begins to depopulate by increasing magnetic field. The model predicts a factor of approximately 2 in the difference of T^* between the fields at which these beats occur. This is close to that observed in Fig. 10. There is, however, a discrepancy in the absolute value of the smearing temperature. Experimentally the smearing occurs approximately a factor of 4 lower than predicted by Eq. (1). However, the calculations are sensitive to the exact potential and density profile close to the antidot and the role of ϕ, the phase coherence length, has not yet been taken into account.[10]

VII. CONCLUSIONS

We have reported low-temperature investigations of a device used to define an artificial impurity. A range of distinct magnetic-field regimes have been considered. At low magnetic fields, the impurity shapes the classical trajectories. At higher fields, when edge states become bound to the impurity, we have identified a transitional regime between nonadiabatic and adiabatic edge-state transport. This regime is characterized by the appearance of resonances related to tunneling through the single electron levels of the bound edge state. These magnetoresistance resonances are accompanied by beat patterns and sharp changes in period and are explained by a model invoking interedge-state coupling. Resonances have

also been generated by changing gate bias. The difference between these oscillations and those generated by sweeping the magnetic field have been explained in terms of lifetime broadening of the bound state. Further experiments are planned to evolve more rigorous models for the many features reported in this paper.

ACKNOWLEDGMENTS

We want to thank M. W. C. Dharma-wardana, D. Loss, and B. Johnson for stimulating discussions, and J. A. Adams, M. Davies, P. A. Marshall, P. Chow-Chong, and R. Barber for assistance in device fabrication.

[1]R. P. Taylor *et al.*, J. Vac. Sci. Technol. B **11**, 628 (1993); Y. Feng *et al.*, Appl. Phys. Lett. **12**, 1666 (1993).

[2]See, also, G. Kirczenow *et al.*, Phys. Rev. Lett. **72**, 2069 (1994).

[3]Y. Aharonov and D. Bohm, Phys. Rev. **115**, 485 (1959).

[4]J. Nixon and J. H. Davies, Phys. Rev. B **41**, 7929 (1990); A. L. Efros, F. G. Pikus, and G. G. Samsonidze, *ibid.* **41**, 8295 (1990).

[5]E. Castaño and G. Kirczenow, Phys. Rev. B **41**, 5055 (1990).

[6]Y. Sun and G. Kirczenow, Phys. Rev. Lett. **72**, 2450 (1994).

[7]C. G. Smith *et al.*, J. Phys. Condens. Matter **1**, 6763 (1989); P. J. Simpson *et al.*, Appl. Phys. Lett. **63**, 3191 (1993).

[8]B. J. van Wees *et al.*, Phys. Rev. Lett. **62**, 2523 (1989).

[9]S. W. Hwang *et al.*, Phys. Rev. B **44**, 13 497 (1991); J. A. Simmons *et al.*, Phys. Rev. Lett. **60**, 1542 (1988); J. K. Jain and S. A. Kivelson, *ibid.* **60**, 1542 (1988).

[10]G. Kirczenow, Phys. Rev. B **50**, 1649 (1994).

[11]M. Büttiker, Semiconduct. Semimet. **35**, 191 (1992).

[12]P. J. Simpson *et al.*, Surf. Sci. **305**, 453 (1994).

[13]A. S. Sachrajda *et al.*, Phys. Rev. B **47**, 6811 (1993); R. P. Taylor *et al.*, Phys. Rev. Lett. **69**, 1989 (1992).

[14]C. J. B. Ford *et al.*, Phys. Rev. B **43**, 7339 (1991).

[15]G. Kirczenow and E. Castaño, Phys. Rev. B **43**, 7343 (1991).

[16]Measurements at the Cavendish Laboratory on a differently fabricated sample have very recently also shown evidence of sharp period changes of the magnetoconductance oscillations corroborating the present findings. C. J. B. Ford (private communication).

[17]As in all mesoscopic systems, the microscopic potential changes when a sample is warmed to 300 K and recooled, due to the repopulation of electron traps; each cooldown yields effectively a new sample.

[18]M. W. C. Dharma-wardana, R. P. Taylor, and A. S. Sachrajda, Solid State Commun. **84**, 631 (1992); A. S. Sachrajda *et al.*, Surf. Sci. **305**, 527 (1994).

[19]J. M. Kinaret and N. S. Wingreen, Phys. Rev. B **48**, 4140 (1993).

[20]I. K. Marmorkos and C. W. J. Beenakker, Phys. Rev. B **46**, 15 562 (1992).

(a)

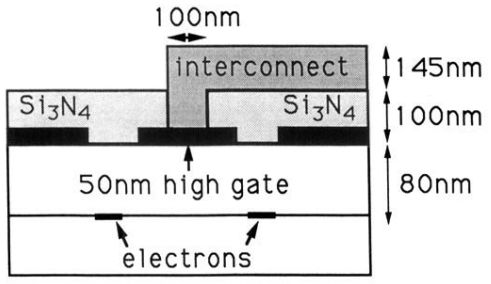

(b)

FIG. 1. (a) A schematic representation of the gate pattern is shown. To contact gate five, we adopt the two-level metallization architecture shown in (b).